Oxide passivated Ni-supported Ru nanoparticles in silica: A new catalyst for low-temperature carbon dioxide methanation

Jaroslaw Polanski [a,*], Tomasz Siudyga [b], Piotr Bartczak [a,e], Maciej Kapkowski [a], Weronika Ambrozkiewicz [a], Agata Nobis [a], Rafał Sitko [a], Joanna Klimontko [c], Jacek Szade [c], Józef Lelątko [d]

[a] Institute of Chemistry, University of Silesia, Szkolna 9, 40-006 Katowice, Poland
[b] Department of Chemistry, Silesian University of Technology, 44-100 Gliwice, Poland
[c] A.Chełkowski Institute of Physics, University of Silesia, Silesian Center for Education and Interdisciplinary Research, 41-500 Chorzów, Poland
[d] Institute of Materials Science, University of Silesia, 75 Pułku Piechoty 1A, 41-500 Chorzów, Poland
[e] NANO-CHEM-TECH, Rewolucjonistów 12/22, 42-500 Będzin, Poland

ARTICLE INFO

ABSTRACT

We tested the catalytic performance of Ni-supported Ru nanoparticles in silica for the first time. The method for supporting Ru nanoparticles on Ni included the formation of nano-Ru/nano-SiO_2, from which silica was digested in the presence of Ni. This provided a nano-Ru/Ni catalyst with an oxide passivation layer on the surface in which unalloyed metallic Ru and Ni were detected. This system, which was tested as a potential methanation catalyst, appears to be highly productive and efficient at low temperature, e.g. ca. 100% conversion can be achieved at ca. 200 °C at a high TOF value of 940 h^{-1}. The longer reaction duration deactivated the catalyst by carbon deposition; however, it did not destroy the catalyst, which could be fully reactivated by hydrogen treatment. In turn, the highest methane productivity (among nano-Re, Rh, Ir or Pd/Ni) given by TOF value of ca. 13855 h^{-1} at higher temperature (460 °C) was observed for the nano-Re/Ni catalyst.

1. Introduction

Carbon is a crucial element in human life and civilization. While organic chemistry demonstrates the engagement of carbon compounds into our lives, carbon dioxide has recently gained much attention. The concentration of CO_2 in the atmosphere has risen from 280 ppm before the industrial revolution to 390 ppm in 2010. This increase has raised concerns about its contribution to the greenhouse effect and the resulting climate changes [1]. Moreover, the predicted amounts of CO_2 that will be emitted by the planet and civilization are important reasons for our concerns about the environment.

On the other hand, CO_2 could be an attractive, renewable, safe and cheap C_1 building block for fuel engineering or organic chemistry. This potential is significantly hindered by the high thermodynamic stability of the CO_2 molecule and therefore new chemistry and technology processes are required. New catalytic methods for CO_2 processing are important challenges that may provide promising strategies. Among such methods catalytic hydrogenation is the one that is most often investigated [2–4]. The most important products from this process could be methanol [5] and methane [6,7].

The methanation of CO_2, which seems to be a relatively simple process, is actually a complex process in the context of mechanistic studies. The issue that is discussed most often is the potential conversion of CO_2 to CO intermediately prior to the methanation itself. Moreover, the kinetics of the processes has not been well established [8–15].

Among the potential catalysts for this process are the metals of the group VIII-XI, of which Ni has probably been investigated most often [16,17]. In this context, CO_2 methanation on Ni has been carefully explored, which has revealed a multistep mechanism that consists of at least six reaction steps in carbon formation and carbon methanation [18]. Ruthenium is another interesting option for the catalytic methanation of the high activity potential. In particular, it has been observed that Ru and Rh prevent carbon sintering and deposition, which makes the catalysts more resistant to deactivation [19–25].

Ni and Ru bimetallic clusters have specifically been prepared and tested as potential catalysts. For example, a remarkable improvement in terms of both the activity and stability of the catalysts were observed in the case of Ni-Ru bimetallics. A series of Ni-Ru/γAl$_2$O$_3$ bimetallic catalysts were prepared while controlling the surface active species to be carefully tested during methanation in the temperature range of 250–500 °C. For the optimal catalysts, the highest conversion (ca. 80%) required ca. 400 °C at which 100% methane selectivity was obseved. This study indicated a complex mechanism of the reaction that depends on the surface species segregation phenomena of metallic Ru and Ru-Ni catalysts [19].

In particular, a low reaction temperature is of key importance in order to follow the advantageous thermodynamics for the exothermic methanation. Lower temperatures prevent also the sintering of the active species. Practically the operation temperature of the catalyst should be below 320 °C, where byproducts of the reverse water-shift gas (RWGS) reaction appear [26] The uniform dispersion of active species over a support of the high surface area was indicated among the most important issues deciding the successful construction of the low temperature catalyst. In this context, recently, the usage of the very high surface area (2961 m^2 g^{-1}) metal–organic framework has been tested as potential support for Ni. The CH$_4$ selectivity was 100% in the range of 200–300 °C, while the conversion reached ca. 75% at 300 °C [17]. In practice, the lowest operation temperature for the catalytic methanation was reported for the Ru catalyst, namely, the Ru/TiO$_2$ system where Ru NPs were assembled on the support using a polygonal barrel-sputtering method with operating temperature at 160 °C. At the same time the analogous Ru/TiO$_2$ catalyst prepared by the wet method needed about 100 °C higher reaction temperature, i.e., ca. 260 °C [27].

Over the past few years, a number of techniques have been developed for the production of nanosized metallic particles and their distribution on different carriers. The methods that have recently been used, which are based on the "bottom-up" and the "top-down" approaches, still have some disadvantages, including broad nanoparticle size distributions and a tendency to aggregate or to form clumps [28,29]. To minimize these problems, we have recently developed a novel, method for the formation of a variety of nanocatalysts that were obtained by digesting nano-SiO$_2$ supported metallic nanoparticles. This appears to be highly efficient in Sonogashira coupling [30], glycerol oxidation [31] or ammonia cracking [32]. The chemical and physical properties of single metal systems can be significantly modified and/or improved by combining metals. Moreover, in nanocatalysis, a variety of the specific interactions of metallic nanoparticles with coatings and supports have been identified [33]. In this study, we show for the first time that Ni grains, when used as a carrier for the deposition of the Ru nanoparticles in the silica, provide highly active unalloyed bimetallics that are extremely active in low-temperature carbon dioxide methanation. Namely, we observed as high as a 100% highly selective conversion at ca. 200 °C with the reaction onset at ca. 150 °C, which compares favorably to all of the previously data reported for the wet preparation protocols [27]. On the other hand, the catalyst appear not only active but also highly resistant to the surface deactivation by coal deposition at the operation temperature. The high activity, stability and economic value of the new nanocatalyst that was obtained are especially worth mentioning. In particular, high cost of Ru is an important obstacle that prevents its application. Therefore, nano-ornamentation with Ru provides a catalyst that has a high surface but low overall bulk Ru concentration.

2. Experimental

2.1. Preparation of Ru$_{NPs}$ on Ni

We prepared Ru$_{NPs}$ supported on silica as an auxiliary source of nanoparticles. Silica was prepared using the Stöber method [34] with tetraethyl orthosilicate (TEOS), which was added to a mixture of ethanol and an aqueous ammonia solution. After silica separation, a solution of a ruthenium precursor (RuCl$_3$) was added. The mixture was sonicated, then concentrated, dried and reduced under
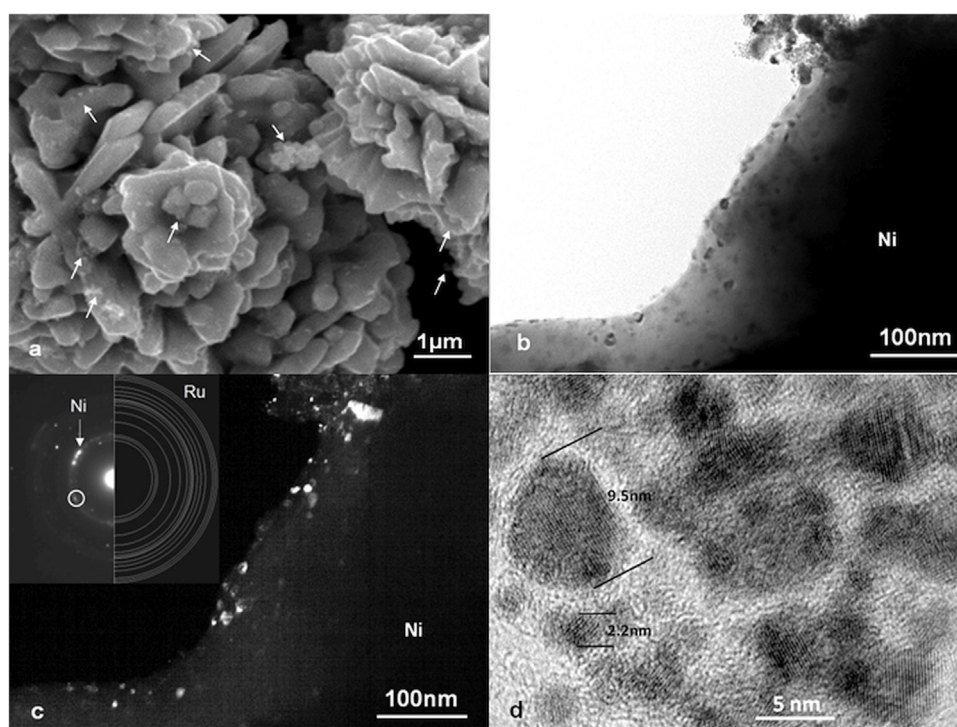

Fig. 1. Structure of silica supported Ru NPs in 1.5% Ru/Ni catalyst. **a**) – SEM image, **b** – **c**) – bright and dark field of TEM images and **d**) – HRTEM image of Ru nanoparticles.

hydrogen at 500 °C. In a typical procedure, 800 mL of anhydrous ethanol and 135 mL of 25 wt.% solution of ammonia were mixed with 78 mL of deionized water. After 10 min of stirring, 60 mL of tetraethyl orthosilicate was added to the reaction mixture, which was next stirred for 3 h at room temperature. The colloidal silica suspension that was obtained was centrifuged, washed to neutral pH (deionized water) and suspended in deionized water (20 mL) in an ultrasound bath and stirred for 90 min. A solution containing the ruthenium precursor (445 mg ruthenium(III) chloride hydrate for 1.0% Ru/SiO_2–Sigma Aldrich) in deionized water (30 mL) was added dropwise into the colloidal silica suspension and mixed in an ultrasound bath for 30 min. Next, it was dried to a constant weight at approx. 90 °C, ground and sieved. The reduction was conducted in an oven under hydrogen at 500 °C for 4 h. The size of the Ru nanoparticles determined from the TEM images was in the range of 3 ÷ 32 nm (supplementary information).

A bimetallic Ru_{NPs}/Ni catalyst was prepared using a novel facile approach that involved the transfer of the nanoparticles from the intermediate carrier, i.e. SiO_2 to the target carrier Ni (Sigma Aldrich). The general method includes several steps. The target carrier, i.e. Ni, (0.985 g) and Ru_{NPs} of a low polydispersity were deposited on the intermediate carrier i.e. 1.0% Ru_{NPs}/SiO_2, (1.50 g), Then this was suspended in deionized water (100 mL) under mechanical stirring and sonication. After 10 min of vigorous stirring, sodium hydroxide (40 mL 40% w/w) was added to the suspension and stirring was continued for 4 h at 80 °C, whereupon the suspension was allowed to stand for about 18 h until the suspended solids sedimented. The suspension was centrifuged and the supernatant was decanted, and then the precipitate was washed in deionized water and centrifuged again to achieve a neutral pH of the supernatant. The precipitate was washed with deionized water once again, centrifuged and the supernatant was removed. The catalyst that was obtained was dried in an electric dryer at 110 °C to a constant weight (1.5% Ru/Ni). This method provided also other systems as listed in Table 2.

2.2. Methods of catalysts characterization

The resulting preparations of silica and mono-, bi-, trimetallic silica or nickel-supported catalysts were examined using X-ray photoelectron spectroscopy (XPS) with a Prevac/VGScienta photoelectron spectrometer. Monochromatic AlKα x-ray radiation ($h\nu = 1486.7$ eV) was used to obtain the photoelectron spectra of the core levels of particular elements. The structure of the XPS multiplets that were obtained was analyzed using the Multipak program from Physical Electronics. Alternatively, the samples were suspended in ethanol, sonicated for 15 min and the resulting materials were deposited on carbon adhesive tape for the preparation of the samples for TEM analyses. The transmission electron microscopy images of the resulting composites were obtained using a JEOL high resolution (HRTEM) JEM 3010 microscope with EDS systems for microanalysis of the chemical composition. A JSM 6480 scanning electron microscope (SEM) was used to investigate the morphology, size of the nanoparticles and distribution on the surface of Ni microparticles of the composite powders. The energy-dispersive X-ray fluorescence (EDXRF) analysis was performed on an Epsilon 3 spectrometer (Panalytical, Almelo, The Netherlands) with an Rh target X-ray tube with 50 μm Be window and max. power of 9 W. The spectrometer was equipped with a thermoelectrically cooled silicon drift detector (SDD) with an 8 μm Be window and a resolution of 135 eV at 5.9 keV. The quantitative analysis was performed using Omnian software and was based on the fundamental parameter method and following measurement conditions: 5 kV, 300 s counting time, helium atmosphere for Si determination; 12 kV, 300 s counting time, helium atmosphere; 50 μm Al primary beam filter (to remove peak of X-ray tube at low-energy region) for Rh

and 30 kV, 120 s counting time, air atmosphere; 100 μm Ag primary beam filter for Ni, Pd, Ru, Re and Ir. The current of the X-ray tube was fixed so that it would not exceed a dead-time loss of ca. 50%. The diffraction experiments (XRD) were carried out using a Panalytical Empyrean X-ray powder diffractometer with Cu K$_\alpha$ radiation (40 kV, 30 mA) that was equipped with a PIXcel detector. Data were collected in the 10°–140° 2θ range at a 0.0131° step. Qualitative phase analysis was performed using the "X'Pert High Score Plus" computer program and the data from the PDF-4 database.

2.3. Methanation

Methanation was performed under atmospheric pressure in a quartz flow microreactor with a fixed catalyst bed with a diameter of 7.5 mm. The feeding gas mixture, 20% CO_2 + 80% H_2, was continuously injected at a flow rate of 3 dm³/h. The CO_2 conversion was determined by analyzing the composition of the tail gas effusing from the microreactor using a thermal conductivity detector-equipped SRI gas chromatograph (1/8 in. diameter, 3 m long column; micropacked with active carbon 80–100 mesh; column temperature of 80 °C with Ar as the effluent gas, 10 dm³ h^{-1}).

3. Results and discussion

3.1. The catalysts design, preparation and structure

Although the design of methanation catalysts in a form of elemental metals or alloys was explored previously [35] according to our knowledge it is a first attempt to design and test unalloyed conjugated polymetallics as potential catalysts for this reaction. In particular, computational screening of potential catalysts for the similar conversion of CO to CH_4 indicated the CO dissociation energy as a useful descriptor of catalytic efficiency. This changes in a sequence Re (ca. −2.0 eV), Ru (0.2 eV), Ni (0.4 eV) [35]. According to Sabatier's principle the highest activity is associated with an *optimum binding energy of substrates to a catalytic centre, strong enough to do catalysis but not too strong, in order to avoid blocking the centre by undesorbed product* [36]. In fact, the measured activity of the Re, Ru or Ni catalysts obeyed the so-called volcano relation with an optimum binding energy somewhere in the middle of the series. Fairly accurately, the experiments had indicated Ru as the most active material. In turn, if we include metal prices Ni, was suggested as both high activity as well as the lowest price material [35]. Last but not least, Re of the significantly lowest activity is often used as an alloy counterpart preventing surface deactivation by coking [37–39]. Accordingly, we used Re, Ru or Ni for the preparation of the new catalysts in the current study.

Bimetallic Ru/Ni contacts were obtained via the sonication of Ru_{NPs}/SiO_2 and a nickel powder and the subsequent digestion of silica with 40% aqueous NaOH. This was washed with deionized water to neutral pH and dried to provide the final catalyst. This facile and scalable wet chemical procedure allowed us to combine small amounts of the expensive Ru with a less expensive and more convenient Ni support. The morphology and composition of the resulting bimetallic Ru/Ni system were studied using scanning electron microscopy (SEM), transmission electron microscopy (TEM) (Fig. 1**b–d**), X-ray diffraction spectroscopy (XRD) (Fig. 2), X-ray photoelectron spectroscopy (XPS) (Fig. 3) and energy-dispersive X-ray fluorescence spectroscopy (EDXRF) (Fig. 4). In Fig. 1 the structure of the final catalyst with Ru_{NPs} mounted on the Ni surface is presented. The nickel support formed the conglomerates of the plate microparticles (Fig. 1**a**). Ru agregations are visible on the Ni surface. When observed using the TEM tehnique (Fig. 1**b–c**), these form oval shapes. The average sizes of the Ru nanoparticles were determined by analyzing the data from different HRTEM images
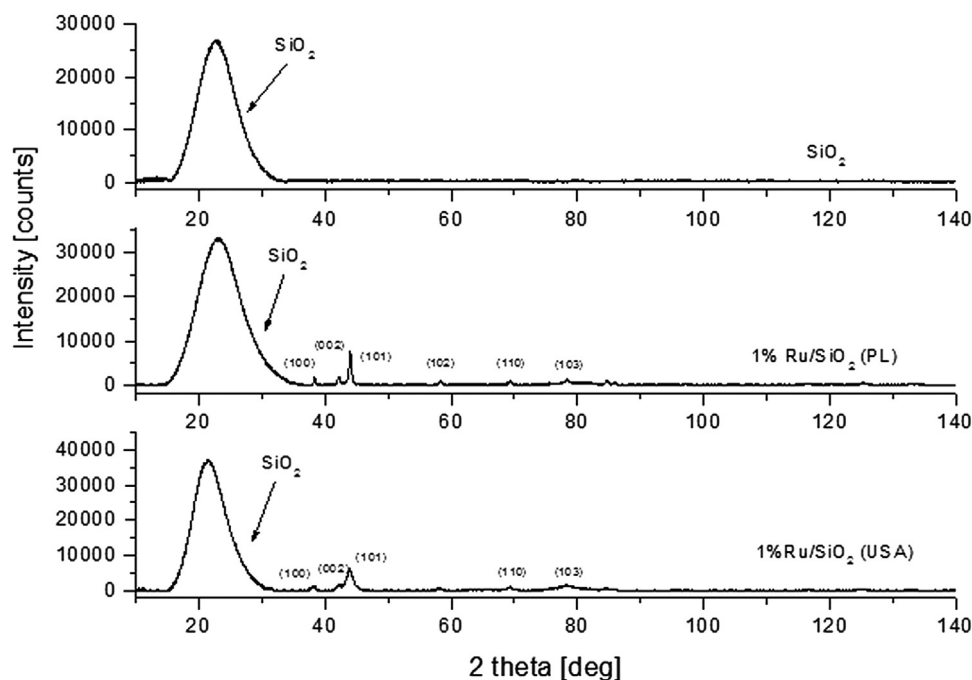
Fig. 2. The X-ray diffraction patterns of 1.0% Ru/SiO$_2$ (USA), 1.0% Ru/SiO$_2$ (PL), and SiO$_2$ samples. Miller indices for experimental peaks of Ru NPs are marked.

Table 1
The size and lattice parameters of nanometal particles determined by XRD technique.

Catalyst	Lattice parameters [Å]	D (nm) Ru
SiO$_2$	–	–
1.0% Ru/SiO$_2$ (Riogen)	a = 2.716 (±0.004) c = 4.292 (±0.002)	3–4
1.0% Ru/SiO$_2$ (PL)	a = 2711 (±0.004) c = 4.289 (±0.003)	10–11

(Fig. 1**d**), which indicated an average diameter of 4.6 ± 1.7 nm. This size is on average lower than a size of the Ru NPs on SiO$_2$ (supplementary materials) which can be explained by deagglomerating effect. Therefore, during NP transfer to the Ni surface the large agglomerates disassemble to the smaller size NPs.

In Fig. 2 the X-ray diffraction of 1.0% Ru/nano-SiO$_2$ (PL) and 1.0% Ru/SiO$_2$ (Riogen USA) is compared to SiO$_2$. Both Ru systems clearly showed peaks that could be attributed to metallic Ru. The broad peak at the low angle range was due to silica. All of the peaks in the XRD spectra were attributed to the pure hexagonal phase (mc) of metallic Ru, as detailed in Table 1. The Scherrer equation was used to estimate the average size of the crystalline particles. Accordingly, the particle size was estimated from the strongest diffraction lines ($2\theta_{100} \sim 38°$, $2\theta_{002} \sim 42°$, $2\theta_{101} \sim 44°$). A comparison of the Ru/nano-SiO$_2$ to that of the commercial Ru/SiO$_2$ (Riogen USA) showed that the size of the NPs that were inversely proportional to the full-with-half-maximum (FWHM) were smaller (3–4 vs. 10–11 nm) in the Ru/SiO$_2$ (Riogen USA) system (Table 1).

The Ru/nano-SiO$_2$ system was obtained as an initial product for the construction of a final catalyst in this study, namely Ru nanoparticles on the Ni support. XPS analysis of the nano-Ru/Ni allowed the chemical composition and the chemical state of the elements constituting the surface of the new catalyst to be determined. Due to the limited inelastic mean free path of photoelectrons, the information was obtained from the topmost atomic layers (4–5 nm depth), which on the other hand, determined the catalytic properties. The atomic Ru/Ni ratio was about 0.3 compared to the 1.44 ± 0.045 wt.%

that was obtained from the much more bulk sensitive EDXRF. This means that the Ru nanoparticles, as expected, were situated on the surface of the Ni grains. Oxygen and carbon and a small amount of silicon, which was connected to the remains of the silica supporting material, were detected as well. Fig. 3 shows the analysis of the most pronounced photoemission lines from Ru and Ni. The Ni 2p$_{3/2}$ line was composed mainly from Ni$_2$O$_3$ with a low intensity contribution from NiO. Surprisingly, the XPS analysis did not detect metallic Ni at the surface but the high intensity satellites that are characteristic for Ni oxides. In addition, Ru showed oxidized state with two doublets that could be attributed to two different oxidation states. While the lower binding energy doublet could be assigned to RuO$_2$, the higher energy doublet could be related with RuO$_3$ or an even higher oxidation state. The literature data are very scarce for Ru oxides and further studies will be necessary to determine the oxidation state. The Ru 3d doublet overlapped with the C 1s line. Fitting showed at least two components that had originated from the carbon that were visible at 285.2 eV (C—C and C—H bonds) and 289.2 eV (C=O bonds).

The EDXRF analysis of studied catalysts revealed intense peaks of the matrix elements (Si Kα, Ni Kα, Ni Kβ at 1.74, 7.48, 8.26 keV, respectively) as well as peaks that corresponded with Rh, Re, Ir, Ru and Pd (Rh Lα, Re Lα, Re Lβ, Ir Lα, Ir Lβ, Ru Kα, Ru Kβ, Pd Kα, Pd Kβ at 2.70, 8.65, 10.01, 9.19, 10.71, 19.28, 21.66, 21.18, 23.82 keV, respectively). The results of the quantitative EDXRF analysis, which was based on fundamental parameter method, are presented in Table 2. An exemplary spectrum of the Ru/Ni catalysts is presented in Fig. 4. Apart from the characteristic peaks of Ni (Ni Kα and Ni Kβ at 7.48 and 8.26 keV, respectively) and Ru (Ru Kα and Ru Kβ at 19.28 and 21.66 keV, respectively), the escape peak at 5.75 keV and sum peaks at 14.96, 15.74 and 16.52 keV were also observed in EDXRF spectrum. This resulted from the high content of Ni and, as a result, a very high intensity of Ni radiation.

In summary, the catalyst structure indicated by the analyses revealed an oxide passivation layer of both Ru and Ni at the catalyst surface. At the same time, metallic Ru was also present in this system.

Table 2

EDXRF analysis of Re, Ru, Rh, Ir and Pd catalysts deposited at SiO_2 or Ni and the N_2 adsorption isotherm in order to calculate the BET surface area.

Catalyst	wt.%					SSA[a] [m²/g]
	Re	Ru	Rh	Ir	Pd	
SiO_2	–	–	–	–	–	241.2
1.0% Re/SiO_2	0.95 ± 0.019	–	–	–	–	277.8
1.0% Ru/SiO_2	–	1.12 ± 0.023	–	–	–	268.1
1.0% Ru/SiO_2[b]	–	1.15 ± 0.031	–	–	–	194.0
0.5% Ru/SiO_2[b]	–	0.57 ± 0.023	–	–	–	188.2
1.0% Rh/SiO_2	–	–	1.14 ± 0.020	–	–	261.9
1.0% Ir/SiO_2	–	–	–	0.98 ± 0.023	–	255.3
1.0% Pd/SiO_2	–	–	–	–	1.14 ± 0.035	248.2
Ni[c]	–	–	–	–	–	104.8
0.2% Re/Ni[c]	0.18 ± 0.007	–	–	–	–	111.3
0.3% Ru/Ni[c]	–	0.32 ± 0.020	–	–	–	136.2
1.5% Ru/Ni[c]	–	1.44 ± 0.045	–	–	–	129.1
1.9% Ru/Ni[c]	–	1.85 ± 0.093	–	–	–	143.5
1.0% RuRe/Ni[c]	0.11 ± 0.023	0.85 ± 0.042	–	–	–	ND[d]
2.0% RuRe/Ni[c]	0.12 ± 0.023	2.08 ± 0.12	–	–	–	ND[d]
1.0% Rh/Ni[c]	–	–	1.19 ± 0.049	–	–	123.7
1.0% Ir/Ni[c]	–	–	–	0.86 ± 0.020	–	138.4
0.5% Pd/Ni[c]	–	–	–	–	0.50 ± 0.014	120.7

[a] Specific Surface Area.
[b] Commercial available catalyst − Riogen®.
[c] Nickel species dimension (Ni support sample) 50 μm.
[d] Not determined.

Table 3

Comparison of activities of CO_2 methanation Re, Ru, Rh, Ir nanoparticles deposited on silica or nickel carrier with literature References.

Entry	Catalyst	T [°C]	TOF [h⁻¹]	Ref.
1	1.0% Ru/SiO_2	381	1208.6	–
2	1.0% Ru/SiO_2[a]	390	1177.1	–
3	0.5% Ru/SiO_2[a]	400	2374.8	–
4	1.0% Re/SiO_2	481	2625.1	–
5	1.0% Rh/SiO_2	493	1208.9	–
6	1.0% Ir/SiO_2	435	2626.9	–
7	1.0% Pd/SiO_2	510	600.1	–
8	1.5% Ru/Ni	204	940.0	–
9	1.5% Ru/Ni	410	1804.6	–
10	0.3% Ru/Ni	245	4320.0	–
11	1.9% Ru/Ni	369	731.7	–
12	1.0% RuRe/Ni	223	1592.5	–
13	2.0% RuRe/Ni	431	650.8	–
14	0.2% Re/Ni	460	13854.7	–
15	1.0% Rh/Ni	477	1158.2	–
16	1.0% Ir/Ni	402	2993.4	–
17	0.5% Pd/Ni	505	2423.0	–
18	Ni	300/500	0/7.8	–
19	4.3% Ni/SiO_2-RHA	500	124.6	[41]
20	4.1% Ni/SiO_2-gel	500	98.0	[41]
21	3.5% Ni/SiO_2-RHA	500	127.1	[40]
22	10.0% Ni/$Ce_{0.5}Zr_{0.5}O_2$	300	786.1	[42]
23	15.0% Ni/TiO_2	218	41.9	[43]
24	0.8% Ru/TiO_2	180	487.3	[27]
25	20.0% Ni/H-Al_2O_3[b]	234	31.4	[44]
26	(10.0% Ni; 1.0% Ru) Ni-Ru/γ-Al_2O_3	350	222.9	[19]
27	2.0% Ru-CeO_2/Al_2O_3	300	2256.0	[45]
28	3.0% Ni/MCM−41[c]	400	503.1	[46]
29	20.0% Ni/MC γ-Al_2O_3	300	117.9	[47]

[a] Commercial available catalyst − Riogen®.
[b] Hierarchical flowerlike Al_2O_3 matrix.
[c] MC mesoporous nanocrystalline γ-Al_2O_3.

3.2. CO₂ methanation

A representative set of the methanation data for the novel catalyst where we presented this as methane yield (conversion degree) vs. tempereature plots are presented in Fig. 5. For the most active catalyst, Ru/Ni system we observed a full 100% conversion degree at temperatures ca. 200 °C, with the reaction onset at ca. 150 °C. Moreover, 100% selectivity was also observed at these points, which means that no other products could have been detected in the reaction system. The activity of the Ru/Ni system clearly exceeded that of the reference material, e.g. pure Ni required ca. 500 °C or Ru/SiO_2 ca. 400 °C to achieve a conversion degree of 100%. Therefore, the activity of the new nanocatalyst compares advanatgeously to the literature data where Ru-Ni bimetllics required 400 °C to achieve an 82.7% conversion with 100% of methane selectivity [19].

In general, a simple direct comparison with the literature data is not possible because the parameters of the reaction, flow and catalyst bed are very rarely reported with sufficient accuracy; however, in Table 3, our results are compared with the data from several literature studies based on the turnover frequency (TOF), a parameter
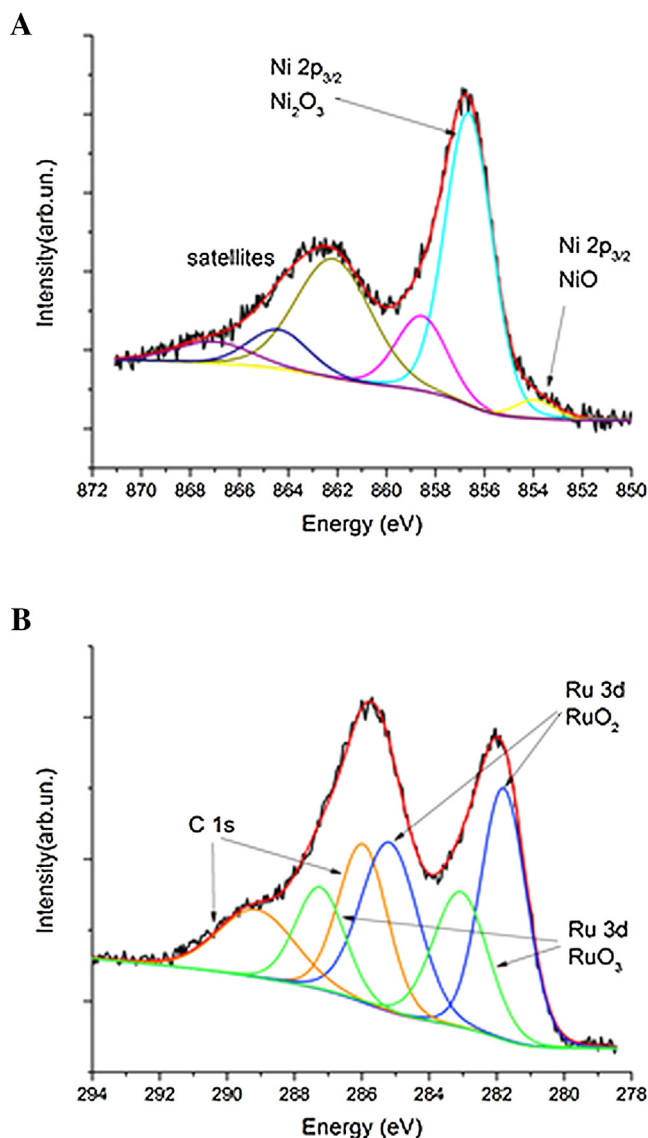
A

B

Fig. 3. XPS photoemission lines from Ru/Ni together with the results of fitting for Ni 2p$_{3/2}$ (**a**) and Ru 3d (**b**).
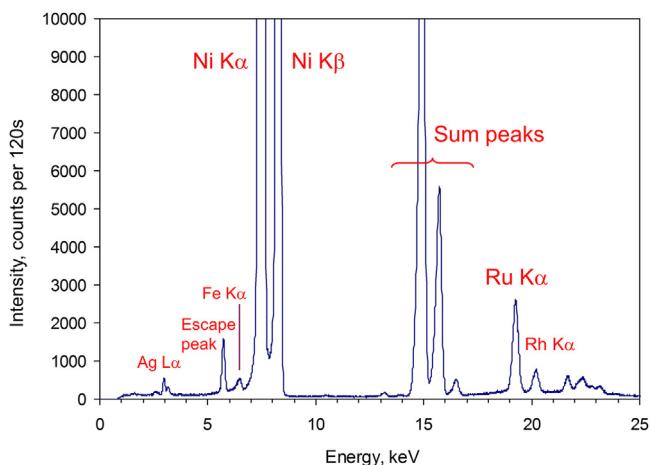

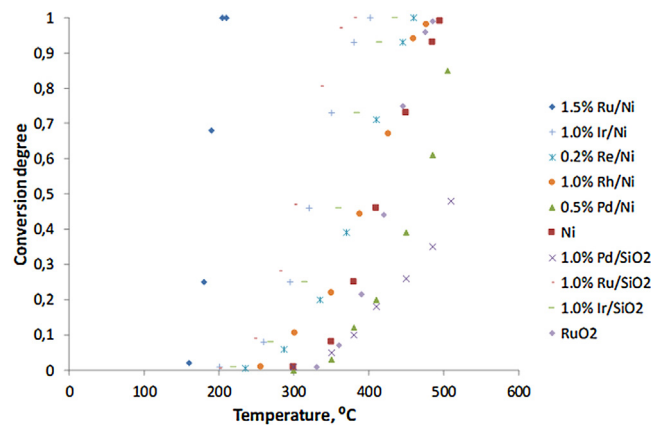**Fig. 4.** Example EDXRF spectrum for 1.5% Ru/Ni catalyst.

Fig. 5. CO_2 conversion of the studied catalysts. The dimension of the nickel species for all catalysts 50 μm (Avantor Performance Materials Poland S.A.).

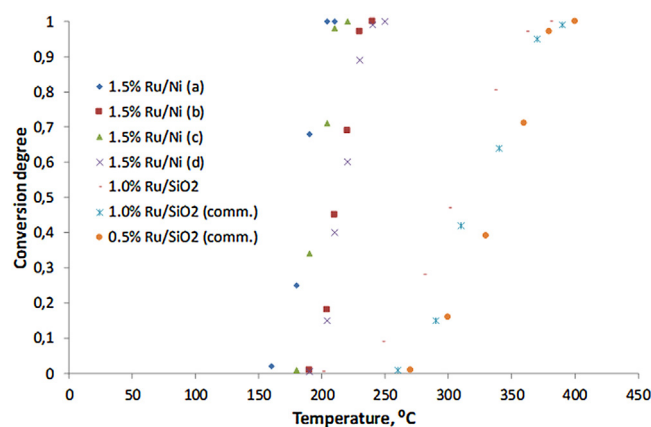**Fig. 6.** The dependence of the conversion degree for the Ru/Ni catalyst on the dimension of the Ni species: **a** − 50 μm (Avantor Performance Materials Poland S.A.), **b** − 5 μm (B&K Bytom, Poland), **c** − 50 μm **d** − 150 μm (Sigma Aldrich).

that allows for a direct comparison of the catalytic measurements performed in various laboratories. All of the reported systems were less reactive than the Ru$_{NPs}$ supported on Ni whose TOF productivity was 940 h^{-1} at 204 °C (Table 3, **entry 8**). It is worth mentioning that at this point, we observed a full 100% conversion to methane. The same system gave a TOF value of 1804.6 h^{-1} at 410 °C (Table 3, **entry 9**) while the most reactive nano-Ru system reported in the literature, Ru/TiO$_2$, gave a TOF productivity of ca. 487 h^{-1} at 180 °C (Table 3, **entry 24**). The increase of the Ru load on the Ni support to 2% (Table 3, **entry 13**) results in the decrease of the catalyst efficiency to ca. 732 h^{-1} at 369 °C. We explain this effect by a fact that apparently the higher nano-Ru loading on the surface do not necessarily appears directly on the surface in a form that is available for the reaction. Moreover, higher metal concentration may result in the agglomeration of the metal which would decrease the activity of the catalyst. Practically, the most active nano-Ru catalyst reported in the literature included ca. 0.8% Ru [27].

The comparison of the activity of the new Ru/Ni catalysts with the other systems, in partcular, the Ru/SiO$_2$ systems is presented in Fig. 5. The nano-Ru/Ni system appeared to be the most active one among all of the catalysts tested. It was interesting to compare the activity of the nano-Ru/SiO$_2$ that was prepared in our study to the commercially available Ru/SiO$_2$. There is a large gap in the reactivity of these systems at low temperatures, i.e. the reaction starts at ca. 200 °C for nano-Ru/SiO$_2$ in comparison to ca. 270 °C for the commercial Ru/SiO$_2$ (Fig. 5 vs. Fig. 6).
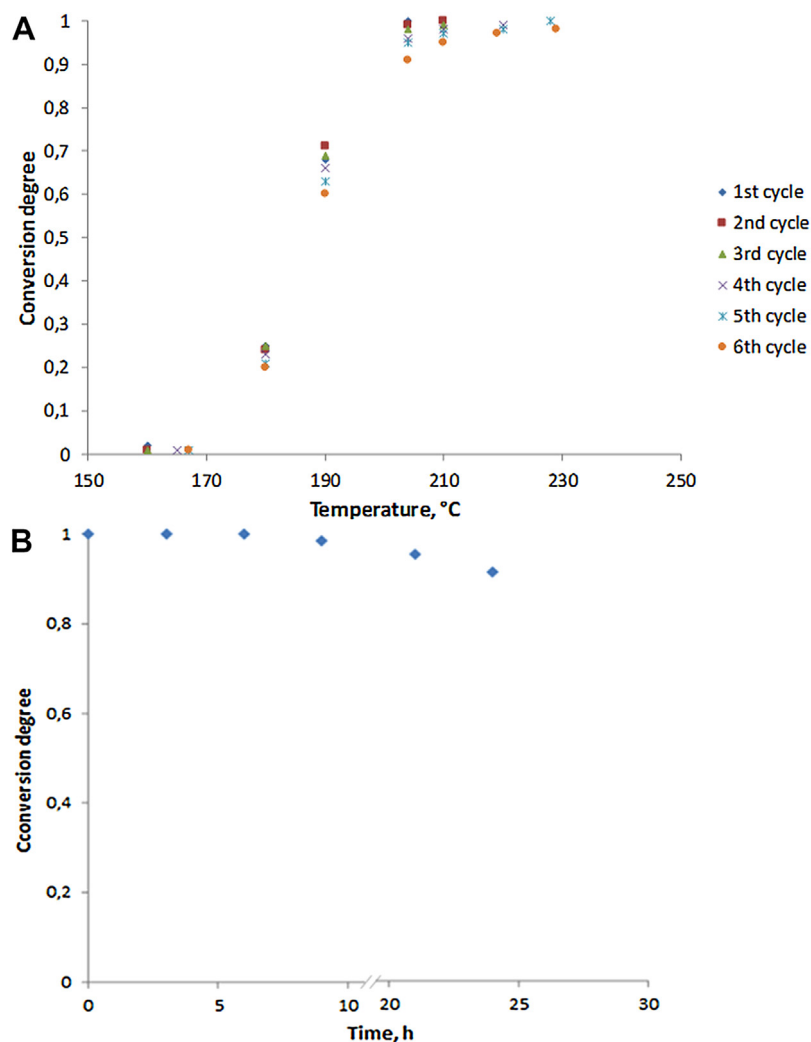
Fig. 7. a: The resistance of 1.5% Ru/Ni catalyst to recycling, shown as the dependence of CO_2 conversion upon the cycle number, **b**: The decrease of the 1.5% Ru/Ni catalyst efficiency during continuous operation.

In Fig. 6 we additionally compared the influence of the Ni support grain size on the activity of the catalyst. This parameter only slightly inflences the reactivity of the system, namely the larger grains (50 μm vs 5 μm) allow us to perform the reaction with higher conversion at slightly lower temperatures. This effect comes probably from the mass transfer limitation which is more important for the smaller grains. It is worth mentioning that the results are highly reproducible even using the samples coming from the different producers (Avantor vs. Sigma-Aldrich).

The stability behavior of the new catalyst is presented in Fig. 7**a and b**. This indicates (Fig. 7a) that the nano-Ru/Ni catalyst is relatively prone to deactivation at low temperatures up to 230 °C even while multiple recycing. Moreover, at higher (>210 °C) or lower (<170 °C) temperatures the catalyst test reveals more stable results than at the intermediate area. This effect is decided by a fact that the kinetics controls the reaction at intermediate temperatures, while at the highest temperature tested (>210 °C) we observed thermo-dynamic control and at the lowest temperatures the catalyst is unreactive. Thus, in the kinetic area the time needed to fully react the reagent (under a constant flow) was not sufficinet to react a full possible amount of flowing CO_2. The activity sequence at the intermediate area is reasonable, the highest is the cycle number the lower is also the CO_2 conversion. Moreover, the conversion suppresion is largest at 190 °C, i.e, in the medium point of the kinetic area (170–210 °C). In the methanation process which is a carbon rich

system the deactivation is not surprising due to carbon deposition on the catalyst surface; therefore; more extensive deactivativation occurred during the longer processing, e.g. 5 h, even at the relatively low temperature of 204 °C. The deposition of carbon on the catalyst surface is proved by XPS analyses of the catalyst samples after reaction (unshown data). The deactivated catalyst could be fully reactivated by treatment with hydrogen. In typical processing, 0.5 h processing at 400 °C was sufficient for the full reactivation of the catalyst. Several repetitions of the process did not destroy the ability of the catalyst to reactivate. In turn, the continuous operation of the catalyst results in a slight deactivation (Fig. 7b). The TG analysis of the catalyst (supplementary information) after this test indicates a small endothermic dehydration at ca. 100 °C, then, a strong exothermic effect 130–600 °C; up to ca. 400 °C with a small not well defined mass loss, and then with a strong mass growth >400 °C. These effects could be connected first with oxidation of a very small amount of carbon deposit (mass loss) and then metal oxidation (mass growth).

An intereresting point is that surprisingly in the virgin Ru/Ni catalyst system the metals, in particular Ru, are present mostly in a form of oxides. Actually, this does not deactivate high activity of the Ru/Ni system. As however in methanation hydrogen was used, the XPS analysis of the catalyst after reaction shows a dramatic change of the chemical composition and chemical state of Ru. The amount of carbon increased few times while the ratio Ru/Ni decreased.

Interestingly, the amount of metalic Ru is still low, which makes the analysis difficult but one can state that the oxidation state of Ru is lower than before reaction. The Ni 2p photoemission line shows a lower effect – the chemical state of Ni is hardly changed.

Additionally to nano-Ru systems, we have tested here other potential nanocatalytic systems specified in Table 3 or shown in Fig. 5, namely, Re, Rh, Ir or Pd. At low temperatures (i.e., ca. 200 °C) Ru significantly outperforms all other systems investigated. However, at higher temperatures (above 400 °C) Re was the most productive system giving a TOF value of ca. 13855 h^{-1} (Table 3, **entry 14**), which means four- to tenfold improvement in the comparison to any other system. Although analyzing a formula for the TOF calculation we should understand that under constant flow of reagents these increase is first of all the result of the much smaller active metal fraction (Re = 0.2%), this fact deserves special attention. We can explain this probably by the higher Re resistnace to the deactivation by a formation of surface carbonous deposits. However, if we attempted to support nano-Ru by nano-Re, to avoid deactivation by carbon deposition, the efficiency of the catalysts significantly decreased (Table 3, **entries 12, 13**). Therefore, we did not observe positive synergy of unalloyed Ru/Re nanosystems.

4. Conclusions

In summary, we have developed a novel strategy for supporting nanoparticles on metal carriers that allowed us to investigate the interaction of the unalloyed nano-Ru and Ni during catalytic methanation for the first time. In particular, we prepared nano Ru supported on Ni grains. The complex catalyst system that resulted from the procedure included oxide passivation at the catalyst surface. At the same time, pure Ru and Ni metals were also present in the system. This material appears to be a higly efficient, flexible and durable catalyst for methanation of carbon dioxide, which is an important and still unsolved issue in C$_1$ chemistry. It is worth mentioning, that the catalyst preparton appeared fully reproducible, and three different Ni samples coming from different suppliers provided fully comparable catalysts of the comparable structure and activity. Although we observed an accumulation of carbon deposit that deactivated the system, the catalyst activity could be fully recovered by hydrogen treatment.

Acknowledgements

Appendix A. Supplementary data

Supplementary data associated with this article can be found, in the online version, at http://dx.doi.org/10.1016/j.apcatb.2017.01.017.

References

[1] W. Wang, S. Wang, X. Ma, J. Gong, Chem. Soc. Rev. 40 (2011) 3703–3727.
[2] G. Centi, S. Perathoner, Stud. Surf. Sci. Catal. 153 (2004) 1–8.
[3] I. Omae, Catal. Today 115 (2006) 33–52.
[4] P.G. Jessop, F. Joo, C.C. Tai, Coord. Chem. Rev. 248 (2004) 2425–2442.
[5] X.M. Ni, Y.S. Tan, Y.Z. Han, N. Tsubaki, Catal. Commun. 8 (2007) 1711–1714.
[6] A. Goguet, F. Meunier, J.P. Breen, R. Burch, M.I. Petch, A.F. Ghenciu, J. Catal. 226 (2004) 382–392.
[7] K.K. Bando, K. Soga, K. Kunimori, H. Arakawa, Appl. Catal. A 175 (1998) 67–81.
[8] J.L. Falconer, A.E. Zagli, J. Catal. 62 (1980) 280–285.
[9] G.D. Weatherbee, C.H. Bartholomew, J. Catal. 77 (1982) 460–472.
[10] D.E. Peebles, D.W. Goodman, J.M. White, J. Phys. Chem. 87 (1983) 4378–4387.
[11] M. Marwood, R. Doepper, A. Renken, Appl. Catal. A 151 (1997) 223–246.
[12] A.L. Lapidus, N.A. Gaidai, N.V. Nekrasov, L.A. Tishkova, Y.A. Agafonov, T.N. Myshenkova, Pet. Chem. 47 (2007) 75–82.
[13] S. Fujita, H. Terunuma, H. Kobayashi, N. Takezawa, React. Kinet. Catal. Lett. 33 (1987) 179–184.
[14] C. Schild, A. Wokaun, A. Baiker, J. Mol. Catal. 63 (1990) 243–254.
[15] J. Sehested, S. Dahl, J. Jacobsen, J.R. Rostrup-Nielsen, J. Phys. Chem. B 109 (2005) 2432–2438.
[16] S. Hwang, J. Lee, U.G. Hong, J.G. Seo, J.C. Jung, D.J. Koh, H. Lim, C. Byun, I.K. Song, J. Ind. Eng. Chem. 17 (2011) 154–157.
[17] W. Zhen, B. Li, G. Lu, J. Maa, Chem. Commun. 51 (2015) 1728–1731.
[18] S.J. Choe, H.J. Kang, S.J. Kim, S.B. Park, D.H. Park, D.S. Huh, Bull. Korean Chem. Soc. 26 (2005) 1682–1688.
[19] W. Zhen, B. Li, G. Lu, J. Ma, RSC Adv. 4 (2014) 16472–16479.
[20] T.A. Milne, R.J. Evans, N. Abatzoglou, J.R. Rostrup-Nielsen, R. Nielsen, Catal. Rev.: Sci. Eng. 46 (2004) 247–270.
[21] E. Akpana, Y. Sun, P. Kumar, H. Ibrahim, A. Aboudheir, R. Idem, Chem. Eng. Sci. 62 (2007) 4012–4024.
[22] D.L. Trimm, Catal. Today 49 (1999) 3–10.
[23] A.L. Kustov, A.M. Frey, K.E. Larsen, T. Johannessen, J.K. Nørskov, C.H. Christensen, Appl. Catal. A 320 (2007) 98–104.
[24] M. Kuśmierz, Catal. Today 137 (2008) 429–432.
[25] C. Crisafulli, S. Scirè, S. Minicò, L. Solarino, Appl. Catal. A 225 (2002) 1–9.
[26] X. Xu, J. Moulijn, Energy Fuels 10 (1996) 305–325.
[27] T. Abe, M. Tanizawa, K. Watanabe, A. Taguchi, Energy Environ. Sci. 2 (2009) 315–321.
[28] H. Skaff, T. Emrick, Nanoparticles: Building Blocks for Nanotechnology, in: V. Rotello (Ed.), Springer Science and Business Media Inc, New York, 2004, p. 32.
[29] J. Kao, K. Thorkelsson, P. Bai, B.J. Rancatore, T. Xu, Chem. Soc. Rev. 42 (2013) 2654–2678.
[30] M. Korzec, P. Bartczak, A. Niemczyk, J. Szade, M. Kapkowski, P. Zenderowska, K. Balin, J. Lełątko, J. Polanski, J. Catal. 313 (2014) 1–8.
[31] M. Kapkowski, P. Bartczak, M. Korzec, R. Sitko, J. Szade, K. Balin, J. Lełątko, J. Polanski, J. Catal. 319 (2014) 110–118.
[32] J. Polanski, P. Bartczak, W. Ambrozkiewicz, R. Sitko, T. Siudyga, A. Mianowski, J. Szade, K. Balin, J. Lełątko, PLoS One 10 (8) (2015) 1–14.
[33] P. Serp, K. Philippot, Nanomaterials in Catalysis, Wiley-VCH, Weinheim, 2013, pp. 168 (173).
[34] K.S. Rao, J. Colloid Interface Sci. 289 (2005) 125–131.
[35] J.K. Nørskov, T. Bligaard, J. Rossmeisl, C.H. Christensen, Nat. Chem. 1 (2009) 37–46.
[36] Emil Roduner, Chem. Soc. Rev. 43 (2014) 8226–8239.
[37] K. Baranowska, J. Okal, Appl. Catal. A 499 (2015) 158–167.
[38] K. Baranowska, J. Okal, N. Miniajluk, Cat. Lett. 144 (2014) 447–459.
[39] S. Koso, Y. Nakagawa, K. Tomishige, J. Catal. 280 (2011) 221–229.
[40] F.W. Chang, T.J. Hsiao, J.D. Shih, Ind. Eng. Chem. Res. 37 (1998) 3838–3845.
[41] F.W. Chang, M.T. Tsay, S.P. Liang, Appl. Catal. A 209 (2001) 217–227.
[42] Q. Pan, J. Peng, T. Sun, D. Gao, S. Wang, S. Wang, Fuel Process. Technol. 123 (2014) 166–171.
[43] J. Liu, C. Li, F. Wang, S. He, H. Chen, Y. Zhao, M. Wei, D.G. Evans, X. Duan, Catal. Sci. Technol. 3 (2013) 2627–2633.
[44] S. He, C. Li, H. Chen, D. Su, B. Zhang, X. Cao, B. Wang, M. Wei, D.G. Evans, X. Duan, Chem. Mater. 25 (2013) 1040–1046.
[45] S. Tada, O.J. Ochieng, R. Kikuchi, T. Haneda, H. Kameyama, Int. J. Hydrogen Energy 39 (2014) 10090–10100.
[46] G. Du, S. Lim, Y. Yang, C. Wang, L. Pfefferle, G. Haller, J. Catal. 249 (2007) 370–379.
[47] S. Rahmani, M. Rezaei, F. Meshkani, J. Ind. Eng. Chem. 20 (2014) 1346–1352.